THE JOURNAL OF PHYSICAL CHEMISTRY A

Article

pubs.acs.org/JPCA

Solvation of Actinide Salts in Water Using a Polarizable Continuum Model

Narendra Kumar[†] and Jorge M. Seminario*[,†,‡,§]

[†]Department of Chemical Engineering, [‡]Department of Materials Science and Engineering, and [§]Department of Electrical and Computer Engineering Texas A&M University College Station, Texas 77843, United States

ABSTRACT: In order to determine how actinide atoms are dressed when solvated in water, density functional theory calculations have been carried out to study the equilibrium structure of uranium plutonium and thorium salts (UO_2^{2+}, PuO_2^{2+}, Pu^{4+}, and Th^{4+}) both in vacuum as well as in solution represented by a conductor-like polarizable continuum model. This information is of paramount importance for the development of sensitive nanosensors. Both UO_2^{2+} and PuO_2^{2+} ions show coordination number of 4−5 with counterions replacing one or two water molecules from the first coordination shell. On the other hand, Pu^{4+}, has a coordination number of 8 both when completely solvated and also in the presence of chloride and nitrate ions with counterions replacing water molecules in the first shell. Nitrates were found to bind more strongly to Pu(IV) than chloride anions. In the case of the Th(IV) ion, the coordination number was found to be 9 or 10 in the presence of chlorides. Moreover, the Pu(IV) ion shows greater affinity for chlorides than the Th(IV) ion. Adding dispersion and ZPE corrections to the binding energy does not alter the trends in relative stability of several conformers because of error cancelations. All structures and energetics of these complexes are reported.

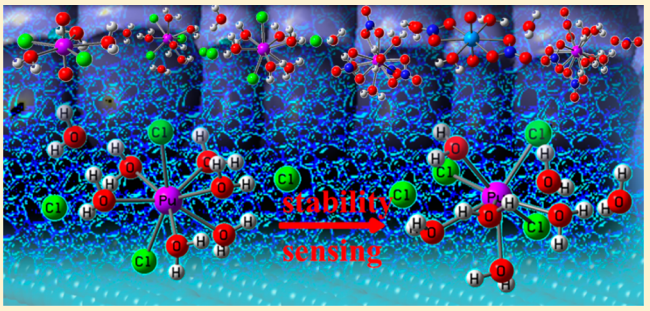

INTRODUCTION

Today 11% of world's electricity production is met through nuclear energy.[1] Although the number of nuclear reactors has declined from decades ago in the U.S. and few other countries, a large number of nuclear plants are being constructed or planned in countries where natural resources such a coal and crude oil are insufficient to meet their rising energy demands. Two-thirds of the 64 units under construction are located in three countries: China, India, and Russia,[1] without considering others in undisclosed locations. Therefore, potential hazards and unforeseen disasters cannot be overlooked. The other important aspect is the growing age of nuclear power plants in operation as indicated in World Nuclear Report 2014.[1] The contamination of groundwater and soil near nuclear processing facilities due to accidental leakage poses a major threat to the environment and human life. Even with the extreme efforts in nuclear safety and safeguards, still our world would need a strong leap in order to reduce to zero the chances of a nuclear accident or of an undesirable nuclear attack. One of the first measures to avoid a colossal loss due to these unwelcome events is to develop very efficient and sensitive nuclear sensor devices in order to catch in the very early stages any potential threat. In this regard, several efforts have been in progress to develop the basic science of nanosensors, which eventually will be able to detect atomistic quantities of fissile materials[2−6] based on the extraordinary properties of new materials such as graphene compounds.[7,8]

In our previous work, we provided a quantum chemistry guided approach to design a nanosensor to detect uranium and plutonium ions which are major constituents in nuclear wastewater.[2] In order to design a fissile nanosensor, the first step is to identify the major radionuclides and their form present in contaminated soil and water near production facilities. Radionuclides such as uranium and plutonium form strong complexes with common counterions such as chlorides, nitrates, carbonates, and sulfates. Ab initio calculations have been widely used to study these complexes; a summary of which has been presented in detail in our previous work.[2] The uranyl (UO_2^{2+}) and plutonyl (PuO_2^{2+}) ions are known to form pentagonal bipyramidal geometries with five water molecules in the equatorial plane. When counterions such as CO_3^{2-}, OH^-, and NO_3^- are present, one or two water molecules in the first shell are replaced by the counterions preserving the 5-fold symmetry. PuO_2^{2+} was found to have a higher affinity for these anions compared to the UO_2^{2+} cation.[9] In addition it was also shown that sulfate ions bound more strongly than nitrate ions.[9] Most of these quantum chemical calculations employ relativistic effective core potential for actinide species and the results obtained are found to compare well with experiments. There have been few studies on aquo-chloro complexes of U(VI) and U(IV) ions in aqueous solution both experimentally[10,11] and theoretically.[12] Using EXAFS spectroscopy, formation of $UO_2(H_2O)_5^{2+}$, $UO_2(H_2O)_4Cl^+$, $UO_2(H_2O)_3Cl_2$, and $UO_2(H_2O)Cl_3^-$ complexes were observed as concentration of chloride ions increases. For U(IV) ions, $U(H_2O)_9^{4+}$, $U(H_2O)_8Cl^{3+}$, $U(H_2O)_{6-7}Cl_2^{2+}$,

Received: July 29, 2014
Revised: December 16, 2014
Published: January 7, 2015

DOI: 10.1021/jp507613a
J. Phys. Chem. A 2015, 119, 689−703

and $U(H_2O)_5Cl_3^+$ complexes were found to occur.[11] On the theoretical side, the structure and energetics of aquo-chloro complexes of UO_2^{2+} were investigated using density functional theory and Car−Parrinello MD.[12] Based on their calculations, they found that monochloride $(UO_2(H_2O)_4Cl^+)$ is five-coordinated, while the trichloride complex $(UO_2(H_2O)Cl_3^-)$ is four-coordinated. The dichloride $(UO_2(H_2O)_nCl_2)$ complex can exist both as four-coordinated or five-coordinated. A lot of effort has been invested on studying the structure and dynamics of uranyl-nitrate complexes as they are the most probable species present in the extraction process of uranium in the PUREX process.[13,14] However, there is a lack of understanding in terms of relative stability of these species and their dissociation in aqueous phase. Using Car−Parrinello molecular dynamics, Wipff et al.[13] showed that the mononitrate-hydrate complex of uranyl binds in a bidentate mode in vacuum with three water molecules in the first shell thus having a coordination number of 5. In aqueous phase, they showed that nitrate preferred to bind in monodentate fashion with four water molecules in the first shell thus preserving CN of 5. They also claimed that, due to low complexation constant between uranyl and nitrates, mononitrate may be the most dominant conformer present in aqueous phase. Classical MD studies done on uranyl-nitrate association in aqueous solution also indicated that nitrates prefer to bind in monodentate fashion with a small quantity of bidentates.[14] However, their study indicates that uranyls are present predominantly in divalent ionic form hydrated by five water molecules. Classical MD simulations were also performed to study the structure of aquo, hydroxyl and carbonate complexes of UO_2^{2+} ion in bulk water and near hydrated quartz surface.[15] Their results indicate that uranyl ions exist in pentagonal bipyramidal symmetry with hydroxide and carbonate ions replacing water molecules in first shell. Carbonates were found to bind in bidentate fashion to the uranyl ion. It is worth mentioning that these classical force fields ignore strong polarization and charge transfer effects present in uranyl complexes. Pu(VI) being a triplet with an electronic configuration of $[Rn]5f^27s^0$ has more diffuse f-orbitals available for binding with ligands unlike U(VI) which is a singlet with a noble gas electronic configuration.

Apart from actinyl complexes, the solvation of Pu^{3+} ion in water was investigated using relativistic DFT to determine binding energies and optimized geometries for several coordination numbers of water molecules.[16] Based on the binding energy of $Pu(H_2O)_n^{3+}$ clusters (n = 6, 8, 9, 10, 12), $Pu(H_2O)_9^{3+}$ had the largest binding energy. Based on total energy, $Pu(H_2O)_8\cdot(H_2O)^{3+}$ was found to be more stable than $Pu(H_2O)_9^{3+}$, the difference in energy being 0.34 eV.[16] The actinides (U^{3+}, Pu^{3+}, and Pu^{4+}) show a higher coordination number of 9−10 with water molecules.[17,18] A significant amount of research has been dedicated to study the hydration of the Th(IV) ion. The first coordination sphere of the Th(IV) ion calculated using B3LYP hybrid functional and relativistic large core effective core potential shows a coordination number of 9 in vacuum.[19] The aqueous phase binding energy was calculated at the optimized geometry in vacuum by adding solvent effects using polarized continuum model. The optimized structure along with ESP charges were then used to obtain second shell of water molecules using hydrated ion concept. In a follow up paper, solvation effects were included in geometry optimization and the coordination number calculated using B3LYP and large core ECP was reported to be 9−10.[20] The bond lengths were similar to the corresponding experimental values for the $Th(H_2O)_9^{4+}$ complex. Ab initio calculations on Th/water complex were also reported using relativistic Douglas-Kroll-Hess Hamiltonian and ANO-RCC basis set. Based on calculated binding energy, their results indicate that $Th(H_2O)_8\cdot(H_2O)_2^{4+}$ is most stable while $Th(H_2O)_{10}^{4+}$ is least stable in vacuum.[21] The hydration structure of $ThCl_4$ and $ThBr_4$ in aqueous solution have also been reported using Car−Parrinello molecular dynamics as well as classical molecular dynamics using polarizable force field.[22] However, unlike the Th(IV) ion, there is a dearth of literature on similar hydration structures for the Pu(IV) ion due to its greater complexity for theoretical treatment as an open-shell ground state.

In this work, our focus is on determining relative stabilities of several salts of UO_2^{2+}, PuO_2^{2+}, and Pu(IV) ions and their speciation in aqueous phase using ab initio density functional theory as they are more abundant in nuclear wastewater. In addition, we have also performed DFT calculations on chloro-complexes of Th(IV) ions. An understanding of solvation chemistry of these ions will allow us to make headway progress in development of nanosensors for these species. The calculation of the most stable structures is relevant for experimental studies on electrochemical response of graphene ribbons to these radionuclides because hydration number and optimized structure of radionuclide complexes will help us to identify their predominant form in nuclear wastewater. It is strongly significant for detection of these radionuclides because they always show up coordinated to these ions in aqueous solution. Hence we are more likely to sense the complex and not the bare ion itself. Knowing this, we can suggest sensor structures and examine their applicability to detect these species in nuclear wastewater. By comparing their relative stabilities, we can assess their likelihood of detection. The stable structures thus obtained will be subsequently used to examine the applicability of graphene-based nanosensor for detection of these species based on changes in the current−voltage characteristics, the methodology of which has been discussed at length in our previous work.[2] The presence of these moieties near the graphene surface causes a change in molecular electrostatic potential of the graphene molecule which can be further transduced into current−voltage curves.

METHODOLOGY

All optimized molecular structures have been obtained using density functional theory[23,24] with the hybrid functional B3PW91. This functional utilizes Becke exchange[25] with some component of Hartree−Fock[26−28] and the correlation functional of Perdew−Wang,[29−33] and has been used successfully in a variety of applications involving nanomaterials,[34−40] nano-biomaterials,[41,42] as well as nanosensors,[43−46] and energetic materials,[47−50] among others. The basis set used for DFT calculations are Stuttgart effective core potential and associated basis set ECP60MWB_SEG for plutonium and uranium.[51,52] For other atoms present in the system, the 6-31G(d) basis set[53] is used unless mentioned otherwise. The ECP parameters for U and Pu have been derived from atomic wave functions obtained using a quasi-relativistic level of theory.[51,52] The Stuttgart small-core scalar relativistic effective core potential, also referred as RECP, has been used widely to study structure of plutonium complexes and has shown good agreement with experimental results. All of the DFT calculations are performed with the program GAUSSIAN-09.[54] The convergence threshold for self-consistent cycle (SCF) to obtain the wave function is set as 10^{-6} for density matrix and 10^{-8} for root-mean-square and maximum density matrix error, respectively. Geometry optimizations are

DOI: 10.1021/jp507613a
J. Phys. Chem. A 2015, 119, 689−703

Table 1. Comparisons of the First and Second Ionization Energies (eV) of Thorium at Several Levels of Theory[a]

basis set	IP I HF	IP I MP2	IP I CCSD(T)	IP I B3PW91	IP II HF	IP II MP2	IP II CCSD(T)	IP II B3PW91	Basis set functions
ECP28MWB	1.90[d]	1.50[e]	5.56[e]	6.08	10.8[d]	11.32[e]	11.56[e]	12.07	8s7p6d4f
ECP28MWB ANO	1.80[d]	2.26[f]	3.46[f]	6.13	10.73[d]	12.21[f]	12.06[f]	11.96	6s6p5d4f3g
ECP28MWB SEG	1.52[f]	2.70[f]	3.11[g]	6.01	10.89[f]	12.10[f]	12.07[g]	12.06	10s9p5d4f3g
ANO-RCC[b]	7.04	6.62		6.04	7.42	9.17		11.93	13s11p10d8f6g3h
expt[c]				6.307				11.9	

[a]Ground state electronic structures reported in literature[51] are Th($^3F_2$) = [Rn]6d^{2}7s^2, Th$^+$($^4F_{3/2}$) = [Rn]6d^{2}7s^1, Th^{2+}($^1G_4$) = [Rn]5f^{1}6d^1. IP I = E(cation) − E(neutral); IP II = E(dication) − E(cation). [b]ANO-RCC uses Douglas-Kroll-Hess second order scalar relativistic calculation. [c]Experimental values.[62] [d]Neutral = quintet; cation = doublet; dication = triplet. [e]Neutral = triplet; cation = doublet; dication = singlet. [f]Neutral = triplet; cation = doublet; dication = triplet. [g]Neutral = singlet; cation = doublet; dication = triplet.

Table 2. Comparisons of the First and Second Ionization Energies (eV) of Uranium at Several Levels of Theory[a]

basis set	IP I HF	IP I MP2	IP I CCSD(T)	IP I B3PW91	IP II HF	IP II MP2	IP II CCSD(T)	IP II B3PW91	basis set functions
LANL2DZ	2.48	3.42	3.57	5.27[e]	13.04	13.46	13.11	10.41[e]	3s3p2d2f
ECP60MWB	−0.28[d]	1.71[d]	2.19	5.55[e]	12.45	13.84	13.43	11.53[e]	8s7p6d4f
ECP60MWB_ANO	3.88	3.61[d]	4.20	5.60[e]	13.32	12.48	13.34	11.53[e]	6s6p5d4f3g
ECP60MWB_SEG	3.22	3.34	3.82	4.93[e]	12.52	12.68	12.76	11.53[e]	10s9p5d4f3g
ANO-RCC[b]	5.27	5.57		5.68	12.26	12.54		11.42	12s10p9d7f5g3h
expt[c]				6.194				10.6	

[a]Ground state electronic structures indicated in literature[51] are U($^5L_6$) = [Rn]5f^{3}6d^{1}7s^2, U$^+$($^4I_{9/2}$) = [Rn]5f^{3}7s^2, U^{2+}($^5I_4$) =[Rn]5f^4. IP I = E(cation) − E(neutral); IP II = E(dication) − E(cation). [b]ANO-RCC uses Douglas-Kroll-Hess second order scalar relativistic calculation. [c]Experimental values.[62] [d]Neutral = triplet; cation = quartet; dication = quintet. [e]Neutral = quintet; cation = sextet; dication = quintet.

carried out with the Berny method[55,56] and the structures are checked to be local minima by running frequency calculations.

The zero-point vibrational corrections were obtained for all optimized structures from the second derivatives calculations. In addition, we have also calculated dispersion corrections using the D3 version of Grimme's empirical dispersion.[57] The uncorrected binding energy (ΔE_u) was calculated as the difference in total energy of complex and total energy sum of its constituent molecules without any correction. The binding energy of each complex was then corrected by adding the zero-point energy correction (ΔZPE) and dispersion corrections (ΔD) to the uncorrected binding energy. In order to study bulk solvent effects, geometry optimizations as well as frequency calculations have also been performed in solution using the Gaussian 09 implementation of the conductor like polarizable continuum model (CPCM).[58,59] The CPCM model places the solute inside a cavity formed by the envelope of spheres using scaled UFF radii centered on the atoms. The molecular surface representing the solute−solvent boundary is chosen as van der Waals surface. The dielectric constant inside the cavity is kept the same as that of vacuum while the dielectric constant of the solvent is used outside the cavity.

RESULTS

Although it is well-understood that there is no way to have a full validation of a level of theory, calculations of real systems for which exists extremely precise experimental information are very valuable to provide some confidence in the selected levels of theory. On the other hand, the calculation of atomic ionization potentials provide a good combination of open shell systems which are considered more difficult to calculate than closed shell systems thus in this sense the test is perhaps the most rigorous. Among several functionals available for DFT calculations, we selected B3PW91 to test it against precise experimental information and, at the same time, decide for a suitable basis set. Therefore, the test is done also with other methods, including few that are usually considered superior to those of DFT. The first and second ionization energies of thorium, uranium, and plutonium were calculated at HF, MP2, CCSD(T), and B3PW91 procedures using several basis sets available for lanthanides and actinides as listed in Tables 1−3. MP2 and CCSD(T) calculations were performed including all electrons due to the fact that a frozen core option results in excessive mixing of frozen core and valence orbitals in the case of ANO-RCC basis set[60,61] obtained from correlated atomic wave functions. This can be due to some of the valence MOs having considerable contribution from the core AOs; therefore, the core MOs need to be considered in the calculation. Among basis sets listed in the Tables 1−3, the ANO-RCC basis set using Douglas-Kroll-Hess second order scalar relativistic calculation performs better than the rest but requires enormous computational resources. On the other hand, Stuttgart effective core potential and associated basis sets yield comparable accuracy at reasonable resource usage.

Thorium, in open shell configuration, shows a strong multireference character. B3PW91 functional results in correct ground state of thorium atom which is a triplet ([Rn]6d^{2}7s^2), while the HF method yields a different triplet [Rn]5f^{2}7s^2 for all three effective core potentials listed in Table 1. Moreover, both MWB60 and MWB60-ANO effective core potential and associated basis sets yield a quintet for thorium atom ([Rn]5f^{1}7s^{1}7p^2) at HF level which is lower in energy than the triplet ([Rn]5f^{2}7s^2) with energy difference of 11.03 and 28.03 kcal/mol, respectively. Similarly, the B3PW91 functional identifies the correct ground state of the Th^{1+} ion, which is a quartet ([Rn]6d^{2}7s^1), while the HF yields a different quartet [Rn]5f^{2}7s^1. In addition, HF results in a doublet ([Rn]5f^{1}7s^2) with lower energy than the quartet [Rn]5f^{2}7s^1. In the case of the Th^{2+} ion, only ANO-RCC basis set yields the correct ground state [Rn]5f^{1}6d^1, while all other basis sets give a different triplet [Rn]5f^{1}7s^1 at both HF and B3PW91 levels with only one exception: the ECP60MWB basis set yields a singlet ([Rn]7s^2), which has lower energy than the triplet ([Rn]5f^{1}7s^1) with energy differences of 18.82 and 11.42 kcal/mol at MP2 and CCSD(T) levels, respectively. The first and second ionization potential of

DOI: 10.1021/jp507613a
J. Phys. Chem. A 2015, 119, 689−703

Table 3. Comparisons of the First Ionization Energy (eV) of Plutonium at Several Levels of Theory[a]

basis set	HF	MP2	CCSD(T)	B3PW91	basis set functions
LANL2DZ	3.76	4.91	4.83	4.85	3s3p2d2f
ECP60MWB	4.78	5.69	5.75	5.71	8s7p6d4f
ECP60MWB_ANO	4.77	5.84	5.82	5.72	6s6p5d4f3g
ECP60MWB_SEG	4.77	5.84	5.82	5.67	10s9p5d4f3g
ANO-RCC[b]	4.73	5.93		5.68	12s10p9d8f5g3h
expt[c]				6.026	

[a]Ground state electronic structures indicated in literature[51] matches with our calculated results: Pu($^7F_0$) = [Rn]$5f^6 7s^2$, Pu^+($^8F_{1/2}$) = [Rn]$f^6 s^1$. IP I = E(cation) − E(neutral); IP II = E(dication) − E(cation). [b]ANO-RCC uses Douglas-Kroll-Hess second order scalar relativistic calculation. [c]Experimental value.[62]

Table 4. Bond Lengths (Å) of UO_2^{2+}, PuO_2^{2+}, and Pu^{4+} Complexes Calculated at the B3PW91/SDD Level of Theory and Comparison with Experimental Values

complex	parameters	in vacuum	in solution	expt[a]
$UO_2(H_2O)_5^{2+}$	U═O	1.74	1.74	1.78
	$U-O_w$	2.47	2.45	2.41
$PuO_2(H_2O)_5^{2+}$	Pu═O	1.70	1.70	1.74
	$Pu-O_w$	2.44	2.42	2.41
$UO_2(NO_3)_2(H_2O)_2$	U═O	1.76	1.76	1.76 ± 0.01
	$U-O_w$	2.53	2.51	2.49 ± 0.02
	$U-O_n$	2.46	2.47	2.45 ± 0.01
$PuO_2(NO_3)_2(H_2O)_2$	Pu═O	1.72	1.72	1.73
	$Pu-O_w$	2.51	2.50	2.43
	$Pu-O_n$	2.45	2.46	2.50
$PuO_2Cl_1(H_2O)_4$	Pu═O	1.76	1.77	1.75
	$Pu-O_w$	2.62	2.59	2.43
	Pu−Cl	2.81	2.98	2.75
$PuO_2Cl_2(H_2O)_3$	Pu═O	1.71	1.72	1.75
	$Pu-O_w$	2.52	2.50	2.49
	Pu−Cl	2.65	2.66	2.70
$Pu(H_2O)_8^{2+}$	$Pu-O_w$	2.41		2.39
$Pu(NO_3)_4(H_2O)_3$	$Pu-O_{w/n}$	2.39−2.51	2.45	2.46
$UO_2Cl_1(H_2O)_4^{1+}$	U═O	1.75	1.75	1.76
	$U-O_w$	2.53	2.49	2.41
	U−Cl	2.57	2.63	2.71
$UO_2Cl_2(H_2O)_3$	U═O	1.75	1.76	1.76
	$U-O_w$	2.54	2.52	2.50
	U−Cl	2.67	2.68	2.73

[a]References 11 and 72−74.

thorium using the B3PW91 functional is calculated to be 6.01 and 12.06 eV, respectively. These are in good agreement with the experimental values[62] of 6.307 and 11.9 eV, respectively.

Resembling thorium, for uranium we observed several single determinant wave functions close in energy to the one of the ground state determinant, depending on the level of theory and basis set employed. Thus, the electronic configuration for uranium is a mixing of few determinants simply due to their closeness in energies. As long as a level of theory yields correct energies, we can conclude that the leading configuration represents quite well the real wave function, which are bypassed anyway by DFT when using the electronic density. We considered two or more spin states for each of the bare ions, UO_2^{2+}, PuO_2^{2+}, Pu^{4+}, and Th^{4+}, in order to find their lowest energy spin-state and we also showed in our earlier work[2] that the lowest energy spin state of their complexes is the same as that of the bare ion.

Only ANO-RCC basis set at HF results in the correct ground state of uranium atom which is a quintet ([Rn]$5f^3 6d^1 7s^2$) while all other methods/basis sets yield a different quintet state. This is the reason for negative or very low ionization energy listed in Table 2. The B3PW91 functional yields the [Rn]$5f^4 7s^2$ quintet for all basis sets used. ECP60MWB and ECP60MWB-ANO basis sets yield a triplet excited state [Rn]$5f^1 6d^3 7s^2$ at HF level, which is lower in energy than the corresponding quintet state [Rn]$5f^2 6d^2 7s^2$.

For the U^{1+} ion, all the listed basis sets, including LANL2DZ, result in the correct quartet ground state [Rn]$5f^3 7s^2$ at the HF level; however, the B3PW91 functional yields a sextet [Rn]$5f^4 7s^1$ with a lower energy than the one corresponding quartet [Rn]$5f^3 7s^2$; with an energy difference between 6.6 and 10.9 kcal/mol, using several ECP basis sets. The U^{2+} ion was always found to be quintet [Rn]$5f^4$ as reported in earlier published work.[51] The first and second ionization potentials of uranium using the B3PW91 functional are calculated to be 5.27 and 11.19 eV, respectively. The experimental values for IP I and IP II are 6.19 and 10.6 eV, respectively.

The ground state of plutonium atom is calculated to be a septet [Rn]$5f^6 7s^2$, while that of singly ionized ion Pu^{1+} is found to be an octet [Rn]$5f^6 7s^1$ at both HF as well as B3PW91 level of theory,

DOI: 10.1021/jp507613a
J. Phys. Chem. A 2015, 119, 689−703

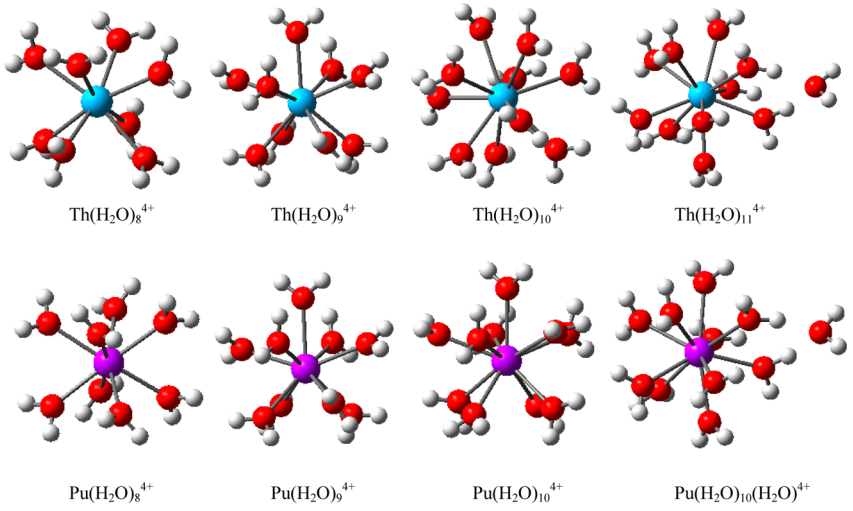

Figure 1. Optimized structures of Th(IV) and Pu(IV) hydrates using B3PW91 functional. Th (cyan), O (red), Pu (magenta), and H (white).

Table 5. Bond Lengths and Binding Energies[a] of Th(IV) and Pu(IV) Hydrates Using B3PW91 Functional in Vacuum[b]

complex	M−O_w (Å)	E	ΔE_u	ΔZPE	ΔD	ΔE_c	ΔG^c
$Th(H_2O)_8^{4+d}$	2.49	−1017.83890	−766.6	19.3	−17.9	−765.2	−676.8
$Th(H_2O)_9^{4+}$	2.52 (2.45)	−1094.33458	−808.9	22.2	−22.9	−809.6	−706.9
$Th(H_2O)_{10}^{4+}$	2.57	−1170.80231	−833.7	25.0	−28.7	−837.4	−719.4
$Th(H_2O)_{11}^{4+}$	2.56 (2.46) 4.43 (4.66)	−1247.29433	−873.7	27.6	−30.9	−877.1	−746.7
$Pu(H_2O)_8^{4+e}$	2.41 (2.39)	−1163.97989	−852.1	19.8	−25.9	−858.2	−762.1
$Pu(H_2O)_9^{4+}$	2.44	−1240.46946	−890.6	22.8	−32.1	−900.0	−787.0
$Pu(H_2O)_{10}^{4+}$	2.49	−1316.93531	−914.2	25.1	−38.8	−927.9	−799.1
$Pu(H_2O)_{11}^{4+}$	2.48, 4.37	−1393.43015	−956.0	27.7	−41.0	−969.3	−828.1

[a]Uncorrected binding energy $\Delta E_u = E(Th(H_2O)_n^{4+}) - E(Th^{4+}) - nE(H_2O)$. ΔZPE and ΔD are zero-point energy and dispersion corrections respectively obtained using similar expression as ΔE_u. Corrected binding energy $\Delta E_c = \Delta E_u + \Delta ZPE + \Delta D$. E is expressed in Ha and all others in kcal/mol. [b]Experimental values are given in parentheses. [c]$\Delta G = G(Th(H_2O)_n^{4+}) - G(Th^{4+}) - nG(H_2O)$. [d]Reported bond length using CPMD for $Th(H_2O)n^{4+}$ complex are Th−O_w = 2.46, 2.49, and 2.48 Å for n = 8, 9, and 10, respectively.[22] [e]Reported bond length for $Pu(H_2O)_8^{4+}$ are 2.42 and 2.43 Å in gas phase using B3LYP and PBE functionals.[78]

matching earlier published results.[51] The first ionization potential of plutonium using B3PW91/ECP60MWB_SEG (Table 3) is estimated as 5.72 eV (expt. value 6.03 eV); however, it falls perfectly in the range 5.69−5.74 eV obtained with the same basis set but with state-averaged CASSCF with subsequent multireference averaged coupled-pair functional calculations.[51,52]

The values thus obtained clearly indicate that B3PW91 functional performs better than Hartree−Fock, second-order Møller−Plesset perturbation theory (MP2), as well as CCSD(T) using the same basis set, with ANO-RCC being an exception. Even though the focus of the paper is on large molecules and complexes of some actinides atoms, it is instructive to verify the quality of level of theory when applied to the individual isolated ion components of those molecules and complexes. The ions, when they are part of the complex, carry several of their intrinsic properties to the complex, and therefore a precise reproduction of their individual behavior can be traced back to the properties of the individual ions.

On the other hand, ionization potentials are the only available very precise experimental information for those ions. Our calculations showed that our methods work pretty well when compared to such precise experimental information. With some exceptions, it is our experience that a suitable level of theory could be tested with energies that are different to those we want to evaluate and with very small systems (molecules) as it should properly work with any other related energies and larger systems if a good level of theory is used. As a matter of fact and simply for practical purposes, most levels of theory are tested against standard heats of formation, atomization energies, ionization potentials, and electron affinities of a database of very small molecules with very precise experimental results, and based on these comparisons,[63−71] calculations are used for larger systems. Thus, these comparisons are in line with mainstream procedures and add some sort of validity to our calculations. Therefore, we selected the B3PW91 functional along with the ECP60MWB_SEG basis set for uranium and plutonium to perform further calculations.

In order to determine ground states for neutral species and higher oxidation states, our rule is to calculate higher spin states until we find three consecutive ones in which the energy always increases. As already mentioned in our earlier work,[2] uranium exists predominantly in the form of uranyl (VI) complexes in solution, while plutonium can exist as Pu^{3+}, Pu^{4+}, PuO^+, and PuO_2^{2+}. For plutonium, it is known that the complexation strength increases in the order: Pu(IV) > Pu(VI) > Pu(III) > Pu(V). Therefore, we considered two or more spin states for each of the bare ions (UO_2^{2+}, PuO_2^{2+}, Pu^{4+}, and Th^{4+}) to find the lowest energy spin-state. The ground state multiplicities for UO_2^{2+} and Th^{4+} were found to be singlet, while PuO_2^{2+} was a triplet and Pu^{4+} a quintet.[2] As already discussed, these actinides tend to form strong bound complexes with common counterions

DOI: 10.1021/jp507613a
J. Phys. Chem. A 2015, 119, 689−703

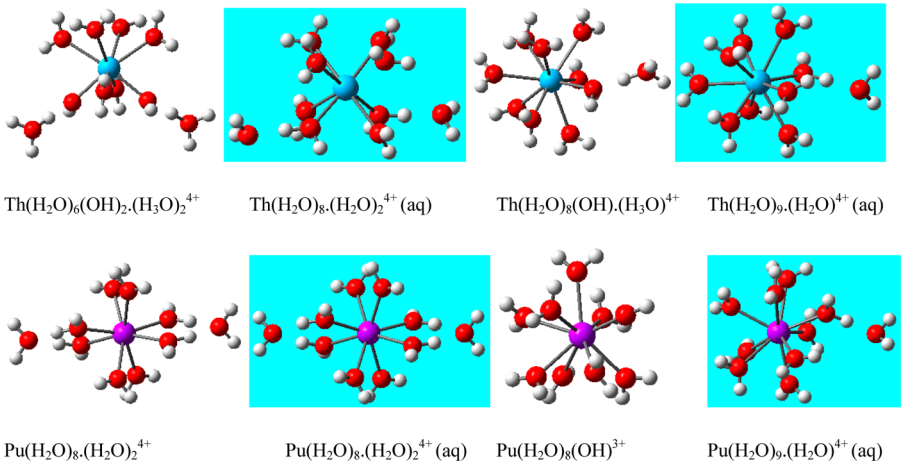

Figure 2. Effect of bulk solvent (CPCM) on coordination number of Th(IV) and Pu(IV) ions. Th (cyan), O (red), Pu (magenta), H (white), and CPCM calculated structures (blue background).

Table 6. Effect of Bulk Solvent on Total Energy of Th/Pu (IV) Hydrates Using CPCM Technique with the B3PW91 Functional[a,b]

complex	E	ΔE_u	ΔZPE	ΔD	ΔE_c	ΔG
		in vacuum				
$Th(H_2O)_6(OH)_2\cdot(H_3O)_2^{4+}$	−1170.84066	−857.7(−820.1)[d]	21.6	−20.7	−856.9	−750.0
$Th(H_2O)_8(OH)\cdot(H_3O)^{4+}$	−1170.82880	−850.3 (−815.3)[d]	23.3	−24.0	−851.1	−739.3
$Th(H_2O)_{10}^{4+}$	−1170.80230	−833.7 (−804.7)[d]	25.0	−28.7	−837.4	−719.4
$Pu(H_2O)_8(H_2O)_2^{4+}$	−1316.98298	−944.1	25.2	−30.4	−949.3	−829.0
$Pu(H_2O)_8(OH)\cdot(H_3O)^{4+c}$	−1317.23577	−1102.8	22.1	−30.2	−1110.8	−1002.2
$Pu(H_2O)_{10}^{4+}$	−1316.93531	−914.2	25.1	−38.8	−927.9	−799.1
		in solution				
$Th(H_2O)_8(H_2O)_2^{4+}$	−1171.80672	−7.0 (12.3)[e]	23.3	−22.5	−6.1	106.3
$Th(H_2O)_9(H_2O)^{4+}$	−1171.80196	−4.0 (0.2)[e]	25.2	−25.6	−4.4	110.5
$Th(H_2O)_{10}^{4+}$	−1171.78943	3.9 (0.0)[e]	24.6	−29.3	−0.8	117.5
$Pu(H_2O)_8(H_2O)_2^{4+}$	−1317.95372	−109.2	25.7	−30.7	−114.2	6.5
$Pu(H_2O)_9(H_2O)^{4+}$	−1317.9414	−101.5	24.1	−34.5	−111.9	12.3
$Pu(H_2O)_{10}^{4+}$	−1317.93232	−95.8	26.7	−39.4	−108.5	21.2

[a] E is expressed in Ha and all others in kcal/mol. See footnotes of Table 5 for nomenclature. [b] The cavity surface area and cavity volume for $Th(H_2O)_n\cdot(H_2O)_{10-n}^{4+}$ are 315.409 Å^2 and 317.416 Å^3 while those for $Th(H_2O)_n\cdot(H_2O)_{10-n}^{4+}$ are 301.939 Å^2 and 306.984 Å^3, respectively. [c] Total energy of hydrolysis products $Pu(H_2O)_8(OH)^{3+}$ and H_3O^+. [d] Values reported in parentheses are from B3LYP calculations published by Yang et al.[19] [e] Values in parentheses are relative energies from B3LYP calculations using CPCM published by Tsushima et al.[20]

present in nuclear wastewater. We also showed in our earlier work[2] that the lowest energy spin state of their complexes is the same as that of the bare ion. We performed geometry optimizations for several uranium(VI) and plutonium (IV, VI) complexes both in vacuum as well as in solution using the CPCM solvation model. The bond lengths thus obtained were compared to experimental data whenever available as shown in Table 4. From these comparisons, we conclude that adding a solvation model improves the estimation of structural parameters, which get closer to experimental values in most cases. We find that DFT usually overpredicts the actinide−water bond by <0.05 Å compared to experimental values. The higher difference in the actinide−chloride bond may be a result of using a smaller basis set 6-31G(d).

A. Structure of First Coordination Shell of Solvated Th^{4+} and Pu^{4+} Ions. We performed ab initio density functional theory calculations using the B3PW91 functional and relativistic small core potential with associated basis set for thorium and plutonium and the 6-311++G(d,p) basis set for O,H atoms to study the hydration of Th^{4+} and Pu^{4+} ions (Figure 1). The bond lengths as well as both corrected and uncorrected binding energy are listed in Table 5. The binding energy was calculated as the difference between energy of optimized $Th(H_2O)_n^{4+}$ and the energy sum of the constituents, and hence, includes the relaxation energy. The corrected binding energy was calculated by including both zero-point vibrational and dispersion corrections. The bond lengths calculated in vacuum are higher by 0.07 Å than those from experiment, 2.45−2.49 Å.[75−77]

Our results indicate a coordination number of 8 being more stable than 9 or 10 for Th^{4+} ions if continuum water (light blue background in Figure 2) is used as inferred from Table 6. In vacuum, we observe hydrolysis effects leading to formation of $Th(H_2O)_6(OH)_2^{2+}$ and $Th(H_2O)_7(OH)^{3+}$ along with hydronium ions compared to stable 10 coordinated structure $Th(H_2O)_{10}^{4+}$. Previous study on the first hydration shell of Th^{4+} at the B3LYP level using a relativistic large core effective core potential[19,20] indicated $Th(H_2O)_{10}^{4+}$ was most stable while $Th(H_2O)_8.(H_2O)_2^{4+}$ least stable and an energy difference of 0.23 kcal/mol between $Th(H_2O)_{10}^{4+}$ and $Th(H_2O)_9(H_2O)^{4+}$ complexes.[20] Spezia et al.[22] used EXAFS and classical molecular dynamics with polarizable force field to show that CN = 9 is the most probable coordination number for Th(IV) ion at diluted conditions in disagreement with our results. A coordination number of 8−10 was reported for $Th(H_2O)_n^{4+}$ experimen-

DOI: 10.1021/jp507613a
J. Phys. Chem. A 2015, 119, 689−703

Table 7. Bond Lengths and Total Energy of Hydrated UO_2^{2+} and PuO_2^{2+} Nitrate Complexes Using the B3PW91 Functional[a]

complex	M−O_w (Å)	M−O_N (Å)	E	ΔE_u	ΔZPE	ΔD	ΔE_c	ΔG
			in vacuum					
$UO_2(NO_3)_2(H_2O)_2$	2.53	2.46	−1340.93304	−590.4	7.4	−10.2	−593.3	−546.2
$UO_2(NO_3)_2(H_2O)_3$	2.53	2.30	−1417.32142	−595.8	10.6	−15.1	−600.3	−539.1
$UO_2(NO_3)_2(H_2O)_2{\cdot}H_2O$	2.50	2.48	−1417.33916	−606.9	10.3	−12.7	−609.4	−550.8
$PuO_2(NO_3)_2(H_2O)_2$	2.51	2.44	−1417.81304	−576.7	7.7	−12.1	−581.2	−530.2
$PuO_2(NO_3)_2(H_2O)_3$	2.51	2.27	−1494.20297	−583.0	10.8	−18.1	−590.3	−524.0
$PuO_2(NO_3)_2(H_2O)_2{\cdot}H_2O$	2.49	2.46	−1494.21804	−592.5	10.5	−14.8	−596.8	−534.2
			in solution					
$UO_2(NO_3)_2(H_2O)_2$	2.51(2.59)[b]	2.47(2.43)[b]	−1340.95447	−96.8	7.2	−10.3	−99.9	−52.8
$UO_2(NO_3)_2(H_2O)_3$	2.48	2.33	−1417.34612	−99.4	9.8	−14.4	−104.0	−44.4
$UO_2(NO_3)_2(H_2O)_2{\cdot}H_2O$	2.48	2.48	−1417.36043	−108.4	9.7	−12.7	−111.4	−53.2
$PuO_2(NO_3)_2(H_2O)_2$	2.49	2.46	−1417.83279	−103.1	7.5	−12.2	−107.8	−58.1
$PuO_2(NO_3)_2(H_2O)_3$	2.47	2.31	−1494.22565	−106.5	10.5	−17.5	−113.5	−49.3
$PuO_2(NO_3)_2(H_2O)_2{\cdot}H_2O$	2.47	2.47	−1494.23785	−114.2	10.2	−14.8	−118.8	−58.0

[a] E is expressed in Ha and all other energies in kcal/mol. See footnotes of Table 5 for nomenclature. [b] U−Ow and U−ON bond lengths reported using CPMD in solution by Bühl et al.[80]

Table 8. Calculated Binding Energy of $UO_2(NO_3)_2(H_2O)_5$ and $PuO_2(NO_3)_2(H_2O)_5$ Clusters Using the B3PW91 Functional[a]

complex	E	ΔE_u	ΔZPE	ΔD	ΔE_c	ΔG
		in vacuum				
$UO_2(NO_3)_2(H_2O)_3{\cdot}(H_2O)_2$	−1570.13582	−630.1	15.6	−20.9	−635.4	−550.5
$UO_2NO_3(H_2O)_2(OH){\cdot}(H_2O)_2HNO_3$	−1570.12467	−623.1	14.8	−18.9	−627.2	−546.5
$UO_2NO_3(H_2O)_3(OH){\cdot}(H_2O)HNO_3$	−1570.12106	−620.9(0.0)[b]	15.1	−20.2	−625.9	−542.2
$UO_2(H_2O)_3(OH)_2{\cdot}(HNO_3)_2$	−1570.10172	−608.7(8.7)[b]	13.1	−20.1	−615.7	−533.1
$PuO_2(NO_3)_2(H_2O)_3{\cdot}(H_2O)_2$	−1647.01578	−616.3	16.4	−25.0	−624.9	−533.6
$PuO_2NO_3(H_2O)_2(OH){\cdot}(H_2O)_2HNO_3$	−1647.00475	−609.4	15.3	−21.6	−615.7	−529.8
$PuO_2NO_3(H_2O)_3(OH){\cdot}(H_2O)HNO_3$	−1647.00084	−607.0	15.5	−23.7	−615.1	−526.0
$PuO_2(H_2O)_3(OH)_2{\cdot}(HNO_3)_2$	−1646.98245	−595.4	14.3	−23.6	−604.8	−516.4
		in solution				
$UO_2(NO_3)_2(H_2O)_3{\cdot}(H_2O)_2$	−1570.16153	−124.9	14.5	−19.8	−130.1	−47.8
$UO_2NO_3(H_2O)_3{\cdot}(H_2O)_2NO_3$	−1570.15414	−120.3	14.4	−18.9	−124.8	−43.3(2.5)[c]
$UO_2NO_3(H_2O)_4{\cdot}(H_2O)NO_3$	−1570.15453	−120.5	14.2	−20.9	−127.2	−43.1(0.0)[c]
$UO_2(H_2O)_5{\cdot}(NO_3)_2$	−1570.13449	−107.9	14.0	−20.3	−114.3	−31.2
$PuO_2(NO_3)_2(H_2O)_3{\cdot}(H_2O)_2$	−1647.04087	−131.9	16.0	−24.2	−140.0	−50.5
$PuO_2NO_3(H_2O)_3{\cdot}(H_2O)_2NO_3$	−1647.03178	−126.2	14.6	−22.0	−133.5	−48.1
$PuO_2NO_3(H_2O)_4{\cdot}(H_2O)NO_3$	−1647.02907	−124.5	15.3	−24.3	−133.4	−44.5
$PuO_2(H_2O)_5{\cdot}(NO_3)_2$	−1647.01392	−114.9	14.9	−24.3	−124.3	−36.6

[a] E is expressed in Ha and all others in kcal/mol. See footnotes of Table 5 for nomenclature. [b] Values in parentheses are relative energy of bidentate and monodentate $UO_2NO_3(H_2O)_4^+$ complex calculated using CPMD in gas phase by Bühl et al.[13] [c] Values in parentheses are relative free energy of bidentate and monodentate $UO_2NO_3(H_2O)_4^+$ complex calculated using CPMD in aqueous phase by Bühl et al.[13]

tally.[75−77] Our results match well with ab initio results at the MP2 level of theory as well as results obtained by molecular dynamics using polarizable force-field done previously to study coordination of Th(IV) ion in aqueous solvent.[21] It was shown that the first hydration shell consists of 8.25 ± 0.2 water molecules.[21] Our results are also in agreement with results obtained using AMOEBA force field where the (8 + 2)-coordination was again shown to have the lowest binding energy among (9 + 1)-coordinated and 10-coordinated structures.[18] Yang et al.[19] reported a 9-coordinated structure having the lowest binding energy in solution phase while the (8 + 2)-coordinated structure having the lowest binding energy in the gas phase. Spezia et al.[79] studied coordination of the Th(IV) ion in water using the single-sweep method coupled with Car−Parrinello molecular dynamics and found that the 9-coordinated structure is the most stable among (8 + 1) and 10-coordinated structures based on change in free energy. Based on free energy calculations, we found that the free energy of the (8 + 2)-coordinated structure is lower than (9 + 1)-coordinated structure by 4.3 and 11.2 kcal/mol lower than the 10-coordinated structure. For aqueous thorium perchlorate solution, Johansson et al.[70] also found a coordination number of 8.0 ± 0.5 with the Th−O_w bond distance of 2.485 ± 0.010 Å using X-ray scattering experiments and also reported that the first shell coordination number was not affected with perchlorate concentration, indicating that perchlorates do not form inner sphere complexes.[70] The difference in binding energy between the (8 + 2)-coordinated and (9 + 1)-coordinated structures is 3 kcal/mol in solution, which is reduced to 1.7 kcal/mol considering ZPE and dispersion corrections.

In the case of the Pu^{4+} ion, $Pu(H_2O)_8.(H_2O)_2^{4+}$ is similarly found to be more stable than $Pu(H_2O)_9.(H_2O)^{4+}$ or $Pu(H_2O)_{10}^{4+}$ complexes when solvation effects are considered. The eight-coordinated complex has a 2.3 kcal/mol lower binding energy than the nine-coordinated complex and a 5.67 kcal/mol lower binding energy than the ten-coordinated complex (Table 6). Molecules in blue background indicate calculations done

DOI: 10.1021/jp507613a
J. Phys. Chem. A 2015, 119, 689−703

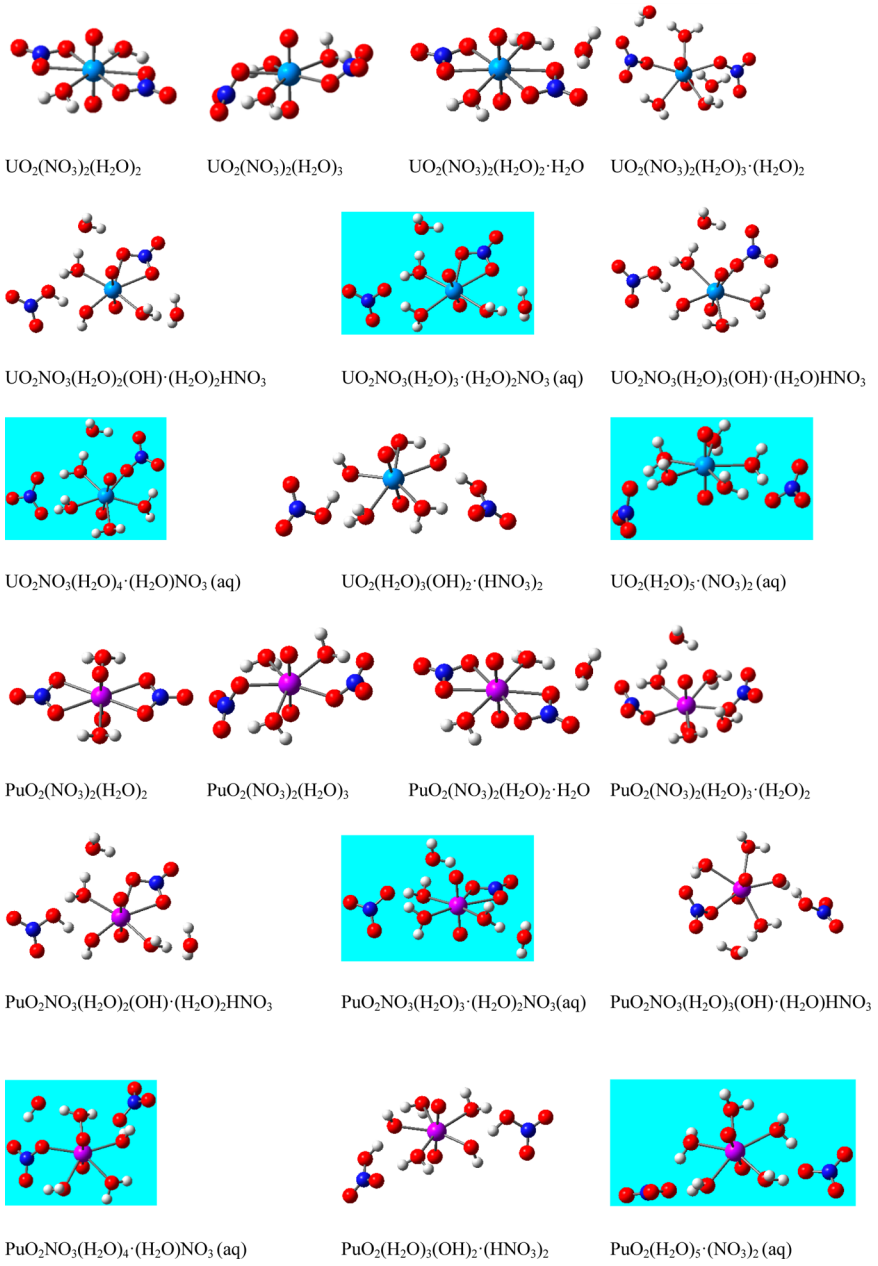

Figure 3. Optimized structures of hydrated UO_2^{2+} and PuO_2^{2+} nitrate complexes using B3PW91 functional. U (blue), O (red), Pu (magenta), N (dark blue), H (white), and CPCM calculated structures (blue background).

using the conductor-like polarizable continuum model.[58,59] In vacuum, we observed formation of hydrolysis products $Pu(H_2O)_8(OH)^{3+}$ and H_3O^+ which repel each other until they are infinitely separated. The energy shown for $Pu(H_2O)_9{\cdot}(H_2O)^{4+}$ is the sum of energy of hydrolysis products. The solvation effects are critical in these cases as they suppress formation of hydrolysis products.

B. Solvation of U(VI) and Pu(IV/VI) Nitrate Complexes. Based on molecular dynamics studies, Ye et al.[14] showed that divalent uranyl ions hydrated by five water molecules in equatorial plane are predominant form in aqueous solution. They also showed that nitrates associate with uranyl cation in monodentate fashion replaced one water molecule each, thus preserving 5-fold co-ordination. Other form of nitrate complexes $UO_2(NO_3)^+$, $UO_2(NO_3)_2$, and $UO_2(NO_3)_3^-$ existed in small fractions which increased with nitric acid concentration. On the contrary Bühl et al.[13] showed using CPMD calculations that the $UO_2(NO_3)_2$ complex with nitrates bonded in bidentate fashion are more stable in aqueous phase. They also observed formation of the $UO_2(NO_3)^+$ complex with five coordination in a monodentate binding mode.[80] Therefore, the role of solvent is critical in studying solvation of these complexes. In a recent experimental work, structure of the plutonyl dinitrate complex $Pu(NO_3)_2(H_2O)_2{\cdot}H_2O$ was studied both in crystalline form and in solution using vis−NIR and Raman spectroscopy.[74] The solution electronic spectrum revealed mononitrate complex domination with negligible dinitrate complex. We carried out DFT calculations on these complexes, both in vacuum and solution phase using CPCM models. Among dinitrate complexes, the $UO_2(NO_3)_2(H_2O)_2{\cdot}H_2O$ complex has a lower binding energy than $UO_2(NO_3)_2(H_2O)_3$ and shows a coordination number of 6 with two nitrates in bidentate mode (Table 7).

DOI: 10.1021/jp507613a
J. Phys. Chem. A 2015, 119, 689−703

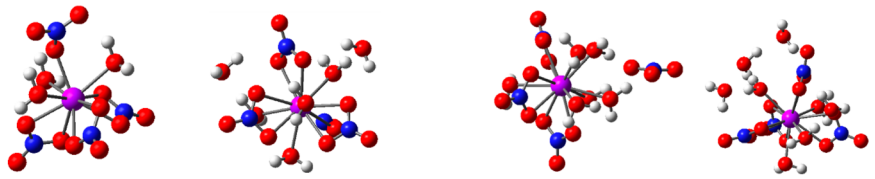

Figure 4. Optimized structures of hydrated Pu(IV) nitrate complexes using B3PW91 functional. Pu (magenta), O (red), N (dark blue), and H (white).

Table 9. Bond Lengths and Total Energy of Hydrated Pu(IV) Nitrate Complexes Using the B3PW91 Functional[a]

complex	Pu−O_W	Pu−O_N	E	ΔE_u	ΔZPE	ΔD	ΔE_c	ΔG
			in vacuum					
$Pu(NO_3)_4(H_2O)_3$	2.51(2.50)[b]	2.39	−1904.26732	−1895.8	13.4	−23.5	−1906.0	−1809.6
$Pu(NO_3)_4(H_2O)_4{\cdot}(H_2O)_2$	2.55	2.49	−2133.47928	−1941.3	22.3	−39.2	−1958.2	−1816.4
$Pu(NO_3)_3(H_2O)_6NO_3$	2.58	2.46	−2133.46148	−1930.1	22.6	−40.8	−1948.4	−1805.0
$Pu(NO_3)_4(H_2O)_4{\cdot}(H_2O)_4$	2.52	2.51	−2286.28062	−1967.4	27.3	−44.9	−1985.0	−1820.2
			in solution					
$Pu(NO_3)_4(H_2O)_4{\cdot}(H_2O)_2$	2.54	2.49	−2133.50655	−285.0	21.5	−38.5	−301.9	−161.9
$Pu(NO_3)_3(H_2O)_6{\cdot}NO_3$	2.57	2.47	−2133.49399	−277.1	22.3	−40.9	−295.7	−152.7

[a]Lengths in Å, E in Ha, and all others energies in kcal/mol. See footnotes of Table 5 for nomenclature. [b]In solution using B3LYP and PBE functionals.[78]

We also studied in detail $UO_2(NO_3)_2(H_2O)_5$ and $PuO_2(NO_3)_2(H_2O)_5$ clusters in order to compare the stability of several conformers. As shown in Table 8, the $UO_2(NO_3)_2$ complex with nitrates in monodentate mode is more stable both in vacuum and solution phase than hydrated mononitrate complex as well as completely solvated $UO_2(H_2O)_5^{2+}$ ions with counterions far from the central ion (Table 8). In vacuum, O−H bonds break forming HNO_3 molecules and OH^- ions bound to the UO_2^{2+} ion in the case of mononitrate and completely solvated nitrate complexes (Figure 3). The difference in binding energy between nondissociated uranyl-nitrate complex and hydrated mononitrate complex is 8.2 kcal/mol (nitrate in bidentate mode) and 9.4 kcal/mol (nitrate in monodentate mode). The difference in binding energy between nondissociated and completely solvated uranyl-nitrate complexes is 19.6 kcal/mol. Thus, nitrate prefers to bind in bidentate mode in the case of the uranyl mononitrate complex in vacuum though the difference in binding energy between monodentate and bidentate is 1.2 kcal/mol only. If we consider the effect of bulk solvents, we do not observe formation of hydroxides though the O−H bond length in water increases up to 1.05 Å. In solution, the difference in energy between nondissociated and hydrated mononitrate complexes reduced to 5.4 kcal/mol for bidentate and 3.0 kcal/mol for monodentate, respectively. This means that monodentate mode is preferred than bidentate mode for mononitrate complex in solution phase; however, based on free energy changes, both are equally probable. If we ignore corrections to binding energy, the difference between monodentate and bidentate mononitrate complex is only 0.2 kcal/mol. The difference in binding energy between nondissociated and completely solvated uranyl-nitrate complexes is 15.8 kcal/mol. We repeat the calculations for PuO_2^{2+} ions as well. Similar behavior is observed for nitrate complexes of PuO_2^{2+}. The $PuO_2(NO_3)_2$ complex with nitrates in monodentate mode are more stable in vacuum as well as solution than hydrated mononitrate as well as completely solvated $PuO_2(H_2O)_5^{2+}$ ions with counterions far from the central ion. The energy difference between nondissociated and hydrated mononitrate complex is 9.2 kcal/mol for bidentate and 9.8 kcal/mol for monodentate complexes; these energies are reduced to 6.5 and 6.6 kcal/mol, respectively, using the solvation model. This means that both monodentate and bidentate are equally favored for the mononitrate complex in solution phase; however, based on free energy changes, bidentate is preferred over monodentate. The difference in binding energy between the nondissociated and completely solvated plutonyl-nitrate complex is 20.1 kcal/mol in vacuum and 15.7 kcal/mol in solution. We observe that including both ZPE and dispersion corrections alters the binding energy by less than ∼2 kcal/mol in above cases.

For the Pu(IV) ion, four nitrates are bonded to the Pu(IV) ion in bidentate mode in first coordination shell. In order to study solvation of $Pu(NO_3)_4$ salt in water, we start by adding water molecules and optimize the structure. We observed that nitrates are very strongly bonded to the Pu(IV) ion and they do not dissociate easily. The coordination number of first shell increases from 10 to 12 (Figure 4) and remains unchanged thereafter on addition of more water molecules to the system. The first coordinate shell can accommodate four water molecules in addition to four nitrates. Any additional water molecule ends up in the second coordination shell. In order to compare the stability of solvated ion, we also optimized the structure of $Pu(NO_3)_3(H_2O)_6{\cdot}NO_3$ and compare its energy with $Pu(NO_3)_4(H_2O)_4{\cdot}(H_2O)_2$. The binding energy of the solvated ion is 9.8 kcal/mol higher indicating nitrates prefer to stay in the first coordination shell (Table 9). When solvent effects are included, the difference in binding energy is reduced to 6.2 kcal/mol, following an expected trend. We further increased the number of water molecules to 8 to obtain second coordination shell of solvent molecules. Our calculations still show no dissociation of nitrates from the central ion. Water molecules in the second shell arrange themselves forming hydrogen bonds with those present in the first shell.

C. Solvation of Pu(IV) and Pu(VI) Chloro Complexes. In this section, we study aquo-chloro complexes of Pu(IV) and Pu(VI) ions. Unlike nitrates, chlorides are weakly bonded to Pu(IV)/(VI) ions. We observe dissociation of counterions with as few as four water molecules during geometry optimization of the Pu(IV) aquo-chloro complex itself. We optimized two

DOI: 10.1021/jp507613a
J. Phys. Chem. A 2015, 119, 689−703

Table 10. Bond Lengths and Total Energy of Pu(IV) and Pu(VI) Chloro Complexes Using the B3PW91 Functional in Vacuum[a]

complex	Pu−O_w (Å)	Pu−Cl (Å)	E	ΔE_u	ΔZPE	ΔD	ΔE_c	ΔG
$PuCl_4(H_2O)_4$	2.50	2.62	−2700.52871	−1900.5	12.1	−20.5	−1908.9	−1825.58
$PuCl_3(H_2O)_4{\cdot}Cl$	2.44	2.54	−2700.52621	−1898.9	11.3	−20.2	−1907.8	−1823.19
$PuO_2Cl_2(H_2O)_3$	2.58(2.55)[b]	2.61(2.67)[b]	−1854.14221	−584.4	8.7	−13.3	−588.9	−536.52
$PuO_2Cl_2(H_2O)_6$	2.47	2.69	−2083.35510	−630.4	16.7	−23.8	−637.6	−547.30

[a]E is expressed in Ha and all others in kcal/mol. See footnotes of Table 5 for nomenclature. [b]Reported bond lengths for $PuO_2Cl_2(H_2O)_3$ in gas phase using B3LYP and PBE functional.[78]

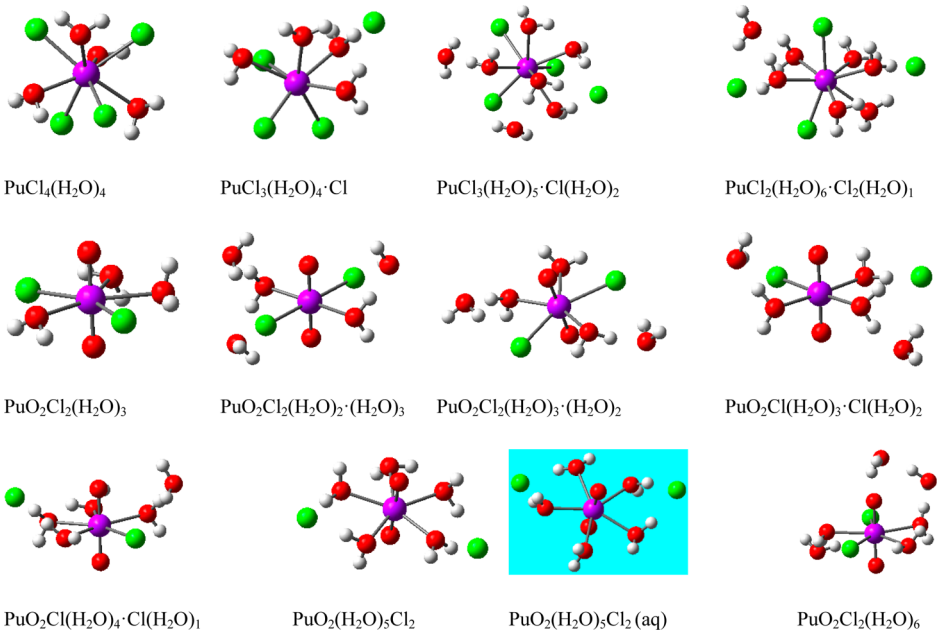

Figure 5. Optimized structures of hydrated Pu(IV) and Pu(VI) chloro complexes using the B3PW91 functional. Pu (magenta), O (red), Cl (green), H (white), and CPCM calculated structures (blue background).

Table 11. Calculated Binding Energy of $PuCl_4(H_2O)_7$ and $PuO_2Cl_2(H_2O)_5$ Clusters Using the B3PW91 Functional[a]

complex	E	ΔE_u	ΔZPE	ΔD	ΔE_c	ΔG
		in vacuum				
$PuCl_4(H_2O)_5{\cdot}(H_2O)_2$	−2929.74804	−1950.6	20.8	−34.2	−1963.9	−1837.3
$PuCl_3(H_2O)_5{\cdot}Cl(H_2O)_2$	−2929.74552	−1949.0	20.6	−35.3	−1963.6	−1835.7
$PuCl_2(H_2O)_6{\cdot}Cl_2(H_2O)_1$	−2929.72409	−1935.5	19.8	−34.9	−1950.6	−1822.7
$PuO_2Cl_2(H_2O)_2{\cdot}(H_2O)_3$	−2006.95861	−619.9	14.5	−21.2	−626.6	−548.0
$PuO_2Cl_2(H_2O)_3{\cdot}(H_2O)_2$	−2006.95125	−615.3	13.9	−19.5	−620.9	−544.3
$PuO_2Cl(H_2O)_4{\cdot}Cl(H_2O)_1$	−2006.93884	−607.5	13.0	−21.5	−616.0	−536.5
$PuO_2Cl(H_2O)_3{\cdot}Cl(H_2O)_2$	−2006.93988	−608.2	13.5	−19.8	−614.4	−537.3
$PuO_2(H_2O)_5Cl_2$	−2006.91764	−594.2	11.1	−21.7	−604.9	−525.4
		in solution				
$PuCl_4(H_2O)_5{\cdot}(H_2O)_2$	−2929.77091	−243.6	19.7	−34.3	−258.3	−132.8
$PuCl_3(H_2O)_5{\cdot}Cl(H_2O)_2$	−2929.78413	−251.9	20.0	−33.4	−265.4	−139.8
$PuCl_2(H_2O)_6{\cdot}Cl_2(H_2O)_1$	−2929.76822	−241.9	19.5	−35.2	−257.6	−129.9
$PuO_2Cl_2(H_2O)_2{\cdot}(H_2O)_3$	−2006.98410	−114.2	13.1	−17.8	−118.9	−46.7
$PuO_2Cl_2(H_2O)_3{\cdot}(H_2O)_2$	−2006.98022	−111.7	13.5	−19.6	−117.8	−41.9
$PuO_2Cl(H_2O)_4{\cdot}Cl(H_2O)_1$	−2006.97649	−109.4	13.2	−21.2	−117.4	−39.7
$PuO_2Cl(H_2O)_3{\cdot}Cl(H_2O)_2$	−2006.97454	−108.2	12.8	−18.1	−113.5	−39.4
$PuO_2(H_2O)_5Cl_2$	−2006.96671	−103.2	12.7	−22.0	−112.6	−33.8

[a]E is expressed in Ha and all others in kcal/mol. See footnotes of Table 5 for nomenclature.

conformers for $PuCl_4(H_2O)_4$. In one case, we found Cl^- leaves the first shell during optimization itself forming $PuCl_3(H_2O)_4^+$ and Cl^- ion, while in other case, all four chloride ions remain bonded to the Pu(IV) ion. The energy difference between the two conformers is however only 1.1 kcal/mol (Table 10). The coordination number of the U(IV) aquo complex has already been reported to be 8−9 in aqueous solution both theoretically[81,82] and experimentally.[11] The combined coordination of N_{Cl}+N_{Ow} in the U(IV) aquo-chloro complex was also reported experimentally to decrease from 9 to 8 with increase in chloride

DOI: 10.1021/jp507613a
J. Phys. Chem. A 2015, 119, 689−703

Table 12. Calculated Binding Energies of $ThCl_4(H_2O)_{10}$ Clusters Using the B3PW91 Functional[a]

complex	Th−Cl (Å)	E	ΔE_u	ΔZPE	ΔD	ΔE_c	ΔG
			in vacuum				
(A)	2.74, 4.17−4.34	−3012.77523	−1883.0	26.1	−40.6	−1897.5	−1735.1
(B)	2.85, 3.81−4.54	−3012.77730	−1884.3	25.8	−38.8	−1897.3	−1737.6
(C)	2.84, 4.26−4.68	−3012.78360	−1888.2	27.5	−39.4	−1900.2	−1738.5
(D)	2.82, 4.30−4.65	−3012.78156	−1887.0	27.1	−39.7	−1899.6	−1737.6
(E)	2.85, 4.29−4.51	−3012.78465	−1888.9	27.8	−41.0	−1902.1	−1737.9
(F)	2.68−2.81, 4.27	−3012.78544	−1889.4	29.0	−39.5	−1899.9	−1739.3
(G)	2.72−2.79, 5.10	−3012.79237	−1893.7	28.6	−39.0	−1904.1	−1744.6
			in solution				
(A)	2.71, 4.40−4.52	−3012.83608	−172.7	26.6	−39.7	−185.7	−25.4
(B)	2.84, 4.08−4.68	−3012.82801	−167.6	26.1	−39.6	−181.2	−20.7
(C)	2.83, 4.41−4.84	−3012.83397	−171.4	26.7	−39.5	−184.2	−23.9
(D)	2.82, 4.44−4.78	−3012.82922	−168.4	26.4	−40.3	−182.3	−21.1
(E)	2.83, 4.47−4.61	−3012.83273	−170.6	28.1	−41.5	−184.0	−19.3
(F)	2.78−2.83, 4.81	−3012.83226	−170.3	27.5	−39.5	−182.3	−22.7
(G)	2.76−2.78, 5.18	−3012.83337	−171.0	27.7	−39.0	−182.3	−22.8
expt[b]	2.8						

[a]E is expressed in Ha and all others in kcal/mol. See footnotes of Table 5 for nomenclature. [b]Expeimental value.[75]

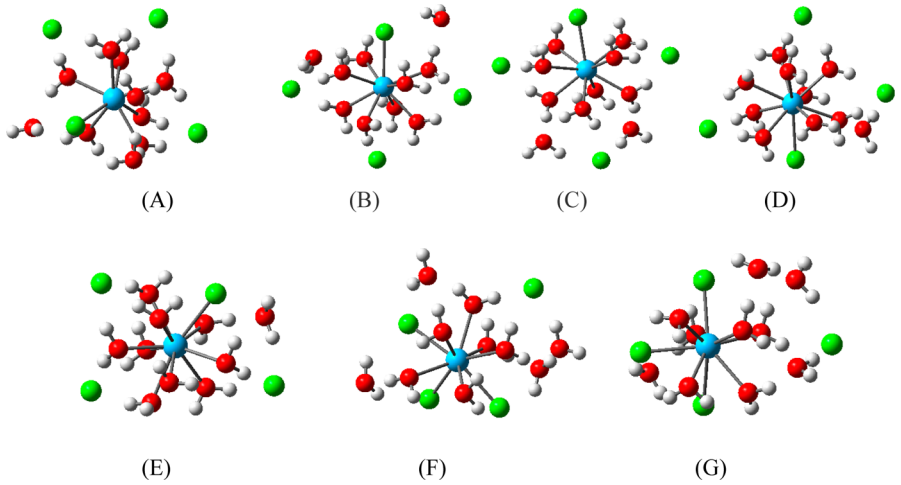

Figure 6. Optimized structures of $ThCl_4(H_2O)_{10}$ clusters using B3PW91 functional. Th (cyan), O (red), Cl (green), H (white). A, B and C have a structural formula of $ThCl(H_2O)_8{\cdot}(H_2O)_2Cl_3$. D and E have a structural formula of $ThCl(H_2O)_9{\cdot}(H_2O)_1Cl_3$. F and G have a structural formula of $ThCl_3(H_2O)_6{\cdot}(H_2O)_4Cl$.

concentration.[11] The coordination number of Pu(IV) aquo complexes was found to be 8 using the continuum model as explained in the previous section. The coordination number for aquo-chloro complexes of Pu(IV) is also found to be 8 with three chlorides present in the first shell as shown in Figure 5. In order to confirm our findings, we also performed a geometry optimization for Pu(IV) aquo-chloro starting with a combined coordination of $N_{Cl}+N_{Ow}$ as 9. The final geometry reverts back to eight-coordination with a water molecule moving out of the first shell. The difference in binding energy between the tetra-chloro complex $PuCl_4(H_2O)_5{\cdot}(H_2O)_2$ and trichloro complex $PuCl_3(H_2O)_5{\cdot}Cl(H_2O)_2$ is only 0.35 kcal/mol, and between the tertra-chloro complex and dichloro complex $PuCl_2(H_2O)_6{\cdot}Cl_2(H_2O)_1$ is calculated to be 13.3 kcal/mol in vacuum. However, using the solvation model, the binding energy of the trichloro complex $PuCl_3(H_2O)_5{\cdot}Cl(H_2O)_2$ is least among the three conformers. The observed trend in binding energy of these complexes remains unchanged if we ignore ZPE and dispersion corrections.

In the case of Pu(VI) chlorides, PuO_2^{2+} retain 5-fold coordination number with two chlorides replacing two water molecules bonded to Pu(VI) ion. In order to study the effect of dilution, we increased the number of water molecules to 6. We observed that chlorides remain bonded to the central cation with the Pu−Cl bond length increasing from 2.49 to2.69 Å (Table 10).

We also obtained the optimized structure of several conformers of $PuO_2Cl_2(H_2O)_5$ to compare their relative stability as shown in Table 11. Among different conformers, $PuO_2Cl_2(H_2O)_2{\cdot}(H_2O)_3$ is the most stable due to the lowest binding energy and $PuO_2(H_2O)_5Cl_2$ is the least stable in vacuum, indicating chlorides prefer to remain bonded to the Pu(VI) ion. On introducing solvation effects, the difference in binding energy between the dichloro complex $PuO_2Cl_2(H_2O)_2{\cdot}(H_2O)_3$ and monochloro complex $PuO_2Cl(H_2O)_4{\cdot}Cl(H_2O)_1$ is reduced to 1.56 kcal/mol. The binding energy of the monochloro complex $PuO_2Cl(H_2O)_3{\cdot}Cl(H_2O)_2$ is however 5.42 kcal/mol higher than the dichloro complex. These results are in line with earlier published Car−Parrinello molecular dynamics simulation[12] of

DOI: 10.1021/jp507613a
J. Phys. Chem. A 2015, 119, 689−703

Table 13. Summary of NBO Contribution Analysis for Common Actinide Complexes

complex	NC[a]	actinide valence	bonds	actinide (%)	$O/O_n/O_w$ (%)
$Th(H_2O)_8^{4+}$	2.27	$7S^{0.16}5f^{0.48}6d^{0.74}7p^{0.29}$	$Th-O_w$	6.7	93.3
$Pu(H_2O)_8^{4+}$	1.81	$7S^{0.19}5f^{4.76}6d^{0.80}7p^{0.35}$	$Pu-O_w$	10.2	89.9
$ThCl_4(H_2O)_7$	−0.04	$7S^{0.30}5f^{0.11}6d^{1.56}7p^{0.01}$	Th−Cl(1)	16.3	83.7
			Th−Cl(2)	4.6	95.4
			Th−Cl(3)	5.1	94.9
			$Th-O_w$	7.8	92.3
$PuCl_4(H_2O)_7$	0.30	$7S^{0.33}5f^{4.91}6d^{1.58}7p^{0.63}$	Pu−Cl	21.0	79.0
$UO_2(NO_3)_2(H_2O)_2{\cdot}H_2O$	1.43	$7S^{0.20}5f^{2.62}6d^{1.44}7p^{0.41}$	$U-O_n$	10.7	89.3
$PuO_2(NO_3)_2(H_2O)_2{\cdot}H_2O$	1.06	$7S^{0.21}5f^{5.14}6d^{1.35}7p^{0.40}$	$Pu-O_n$	12.3	87.8
			$Pu-O_w$	9.7	90.3
$UO_2Cl_2(H_2O)_3$	1.05	$7S^{0.23}5f^{2.71}6d^{1.63}7p^{0.17}$	U−Cl(1)	5.3	94.7
			U−Cl(2)	17.1	82.9
			U−Cl(3)	7.7	92.3
			$U-O_w$	8.5	91.5
$PuO_2Cl_2(H_2O)_3$	0.75	$7S^{0.25}5f^{5.17}6d^{1.53}7p^{0.45}$	Pu−Cl	21.1	78.9

[a]NC, natural charge.

aquo-chloro complexes of U(VI) in aqueous solution where it was shown that $PuO_2Cl_2(H_2O)_3{\cdot}(H_2O)_2$ was stable for a few picoseconds and transform into more stable $PuO_2Cl_2(H_2O)_2{\cdot}(H_2O)_3$ conformer.

D. Solvation of Th(IV) Chloro Complexes. We also optimized five different conformers of $ThCl_m(H_2O)_n{\cdot}(H_2O)_{10-n}Cl_{4-m}$ both in vacuum and in solution as shown in Table 12 and Figure 6. A, B, and C have a coordination number ($N_w + N_{Cl}$) of 9 while D and E are 10-coordinated structures. Conformers F and G are also 9-coordinated structures but with three chlorides in the inner coordination sphere. Based on the binding energy, conformer G $ThCl_3(H_2O)_6{\cdot}Cl(H_2O)_4$ is the most stable than other conformers in vacuum, while in solution conformer A $ThCl(H_2O)_8{\cdot}Cl_3(H_2O)_2$ is the most stable. Moreover, the binding energies of conformers C, D, and F are very similar in vacuum. In solution, C and E have similar binding energies. The binding energies of D, F, and G are also very close which is very interesting due to the fact that D is a 10-coordinated structure with one chloride in the first shell while F and G are 9-coordinated structure with three chlorides in the first shell. Based on the change in free energy, conformer A is the most stable and $\Delta\Delta G$ between conformers A and G is 2.7 kcal/mol in solution. In vacuum, we observe a clear trend for ΔG with conformer G is found to be most stable and $\Delta\Delta G$ between conformers C and G is 6.1 kcal/mol. It can be thus concluded that chlorides remain in the first shell forming an inner sphere complex with the Th−Cl bond length varying between 2.74−2.85 Å in vacuum. The coordination number ($N_w + N_{Cl}$) is found to be 9−10. In solution, our results indicate that one chloride enters the first coordination shell at 2.71−2.84 Å as observed experimentally by Johansson et al.[75] using large angle X-ray scattering measurements. Their experimental results indicate that chlorides tend to form inner sphere complexes, which leads to an increase in coordination number around the thorium ion by addition of a chloride ion to the inner sphere.[75] Recent work done by Spezia et al.,[22] however, found no evidence of chloride in the first shell at low concentration but observed chloride ion in the first shell at a distance of ∼2.9 Å at high concentration. Thus, we can conclude that Pu(IV) ions bind chloride ions more strongly than Th(IV) ions do.

E. Bonding Nature of Actinides with Common Counterions. Based on the simple electronegativity difference between Pu(1.28), O(3.5), and Cl(3.0), the percentages of ionic character of Pu−O and Pu−Cl bonds are 71% and 52%, respectively. Similarly for U(1.38), the percentages of ionic character of U−O and U−Cl bonds are 67% and 48%, respectively. We performed a detailed natural bond order (NBO) analysis on several actinide complexes as shown in Table 13 to understand the nature of bonding present in actinide complexes with common counterions present in nuclear wastewater.

Based on NBO analysis of actinide complexes, we observe formation of covalent bonds between the actinide ion and water as well as counterions present, however, tending toward more ionic character. In the case of the $Th(H_2O)_8^{4+}$ complex, all $Th-O_w$ covalent bonds have very high contribution from water O atoms (93%). In the case of the $Pu(H_2O)_8^{4+}$ complex, we found only four $Pu-O_w$ covalent bonds; however, the contribution from water O atoms was reduced to 90%. In the case of $ThCl_4(H_2O)_7$ and $PuCl_4(H_2O)_7$, relatively stronger covalent bonds are formed between actinide and chloride ions with percentage contribution as high as 16% for Th(IV) and 18% in the case of the Pu(IV) ion. Unlike $ThCl_4(H_2O)_7$, we did not find covalent bonds between Pu(IV) and water O atoms in the case of $PuCl_4(H_2O)_7$.

From NBO analysis performed on the nitrate complex of actinyl species, we found covalent bonds formed between nitrate O atoms and U(VI) or Pu(VI) ions with percentage contribution from U(VI) being 10−11% and from Pu(VI) being 11−12%, respectively. We also found a weak $Pu-O_w$ covalent bond for $PuO_2(NO_3)_2(H_2O)_2{\cdot}(H_2O)$ with 90% contribution from water O atom.

CONCLUSIONS

Density functional theory has been applied to study the structure and solvation of U(VI), Pu(IV), and Pu(VI) using a relativistic small core effective core potential. We found that zero-point vibrational energy corrections to the binding energies cancel with the corresponding empirical dispersion corrections in vacuum with these corrections individually contributing with up to 3% of the binding energy. However, in solution, dispersion corrections can exceed ZPE correction by up to 13% depending upon the size of the molecule; this may be due to the fact that the dispersion correction is not designed for continuum models. We also found that solvent effects are critical in examining the structure of these solvated ions. In vacuum, we observe hydrolysis of the Pu(IV)

DOI: 10.1021/jp507613a
J. Phys. Chem. A 2015, 119, 689−703

ion for nine-coordination which was suppressed on introduction of solvent effects using polarizable continuum model. The eight-coordination was found to be most stable for both Th(IV) and Pu(IV) ions with the nine-coordinated complex being 1.7 and 2.3 kcal/mol higher in energy for Th(IV) and Pu(IV), respectively. In the case of U(VI) nitrate complexes, the $UO_2(NO_3)_2$ complex with nitrates in monodentate mode is more stable both in vacuum and solution phase than the hydrated mononitrate complex as well as completely solvated $UO_2(H_2O)_5^{2+}$ ions with counterions far from the central ion. For the uranyl mononitrate complex, a monodentate mode is preferred than the bidentate mode for the mononitrate complex in solution phase. In the case of PuO_2^{2+}, both monodentate and bidentate are equally favored for mononitrate complex in solution phase. We observed that nitrates are very strongly bonded to the Pu(IV) ion, and they do not dissociate easily and prefer to stay in a first coordination shell. Unlike nitrates, chlorides are weakly bonded to Pu(IV) ions. Pu(IV) ions although have a greater affinity for chlorides than Th(IV) ions in solution. The coordination number for aquo-chloro complexes of Pu(IV) is found to be 8 with three chlorides present in the first shell. In the case of Pu(VI) chlorides, PuO_2^{2+} retains a 5-fold coordination number with two chlorides replacing two water molecules bonded to the Pu(VI) ion. The coordination number for chloro-aquo complexes of Th(IV) (N_w + N_{Cl}) is found to be 9−10, and one chloride enters the first coordination shell at 2.8 Å forming an inner sphere complex. The NBO analysis performed on actinide complexes reveals formation of covalent bonds between actinide ion and water as well as counterions present, but with high ionic character.

AUTHOR INFORMATION

Corresponding Author

*E-mail: seminario@tamu.edu.

Notes

The authors declare no competing financial interest.

ACKNOWLEDGMENTS

We acknowledge the high-performance computing support provided by the Texas A&M Supercomputer Facility and the Texas Advanced Computing Center (TACC) as well as Michael Kaminski from the Argonne National Laboratory's Nuclear Forensics and Nanoscale Engineering Group for discussions on the experimental aspects of radioactive nuclides. We also acknowledge the Argonne National Laboratory's Laboratory-Directed Research and Development Strategic Initiative and the ARO/MURI project W911NF-11-1-0024 for their support.

REFERENCES

(1) Schneider, M.; Froggatt, A., World Nuclear Industry Status Report 2013.

(2) Kumar, N.; Seminario, J. M. Design of Nanosensors for Fissile Materials in Nuclear Waste Water. *J. Phys. Chem. C* **2013**, *117*, 24033−24041.

(3) Romanchuk, A. Y.; Slesarev, A. S.; Kalmykov, S. N.; Kosynkin, D. V.; Tour, J. M. Graphene oxide for effective radionuclide removal. *Phys. Chem. Chem. Phys.* **2013**, *15*, 2321−2327.

(4) Sun, Y.; Shao, D.; Chen, C.; Yang, S.; Wang, X. Highly Efficient Enrichment of Radionuclides on Graphene Oxide-Supported Polyaniline. *Environ. Sci. Technol.* **2013**, *47*, 9904−9910.

(5) Foxe, M.; Cazalas, E.; Lamm, H.; Majcher, A.; Piotrowski, C.; Childres, I.; Patil, A.; Chen, Y. P.; Jovanovic, I. In *Graphene-based neutron detectors*, Nuclear Science Symposium and Medical Imaging Conference (NSS/MIC), 2011 IEEE, 23−29 Oct. 2011; 2011; pp 352−355.

(6) Patil, A.; Koybasi, O.; Lopez, G.; Foxe, M.; Childres, I.; Roecker, C.; Boguski, J.; Gu, J.; Bolen, M. L.; Capano, M. A., et al. In *Graphene field effect transistor as radiation sensor*, Nuclear Science Symposium and Medical Imaging Conference (NSS/MIC), 2011 IEEE, 23−29 Oct. 2011; 2011; pp 455−459.

(7) Geim, A. K.; Novoselov, K. S. The rise of graphene. *Nat. Mater.* **2007**, *6*, 183−191.

(8) Huang, X.; Yin, Z.; Wu, S.; Qi, X.; He, Q.; Zhang, Q.; Yan, Q.; Boey, F.; Zhang, H. Graphene-Based Materials: Synthesis, Characterization, Properties, and Applications. *Small* **2011**, *7*, 1876−1902.

(9) Craw, J. S.; Vincent, M. A.; Hillier, I. H.; Wallwork, A. L. Ab Initio Quantum Chemical Calculations on Uranyl UO_2^{2+}, Plutonyl PuO_2^{2+}, and Their Nitrates and Sulfates. *J. Phys. Chem.* **1995**, *99*, 10181−10185.

(10) Allen, P. G.; Bucher, J. J.; Shuh, D. K.; Edelstein, N. M.; Reich, T. Investigation of Aquo and Chloro Complexes of UO22+, NpO2+, Np4+, and Pu3+ by X-ray Absorption Fine Structure Spectroscopy. *Inorg. Chem.* **1997**, *36*, 4676−4683.

(11) Hennig, C.; Tutschku, J.; Rossberg, A.; Bernhard, G.; Scheinost, A. C. Comparative EXAFS Investigation of Uranium(VI) and -(IV) Aquo Chloro Complexes in Solution Using a Newly Developed Spectroelectrochemical Cell. *Inorg. Chem.* **2005**, *44*, 6655−6661.

(12) Bühl, M.; Sieffert, N.; Golubnychiy, V.; Wipff, G. Density Functional Theory Study of Uranium(VI) Aquo Chloro Complexes in Aqueous Solution. *J. Phys. Chem. A* **2008**, *112*, 2428−2436.

(13) Bühl, M.; Diss, R.; Wipff, G. Coordination Mode of Nitrate in Uranyl(VI) Complexes: A First-Principles Molecular Dynamics Study. *Inorg. Chem.* **2007**, *46*, 5196−5206.

(14) Xianggui, Y.; Smith, R. B.; Shengting, C.; De Almeida, V.; Khomami, B. Influence of Nitric Acid on Uranyl Nitrate Association in Aqueous Solutions: A Molecular Dynamics Simulation Study. *Solvent Extr. Ion Exch.* **2010**, *28*, 1−18.

(15) Greathouse, J. A.; O'Brien, R. J.; Bemis, G.; Pabalan, R. T. Molecular Dynamics Study of Aqueous Uranyl Interactions with Quartz (010). *J. Phys. Chem. B* **2002**, *106*, 1646−1655.

(16) Blaudeau, J.-P.; Zygmunt, S. A.; Curtiss, L. A.; Reed, D. T.; Bursten, B. E. Relativistic density functional investigation of $Pu(H_2O)_n^{3+}$ clusters. *Chem. Phys. Lett.* **1999**, *310*, 347−354.

(17) Duvail, M.; Martelli, F.; Vitorge, P.; Spezia, R. Polarizable interaction potential for molecular dynamics simulations of actinoids-(III) in liquid water. *J. Chem. Phys.* **2011**, *135*, 044503−044510.

(18) Marjolin, A.; Gourlaouen, C.; Clavaguéra, C.; Ren, P.; Wu, J.; Gresh, N.; Dognon, J.-P.; Piquemal, J.-P. Toward accurate solvation dynamics of lanthanides and actinides in water using polarizable force fields: from gas-phase energetics to hydration free energies. *Theor. Chem. Acc.* **2012**, *131*, 1−14.

(19) Yang, T.; Tsushima, S.; Suzuki, A. Quantum Mechanical and Molecular Dynamical Simulations on Thorium(IV) Hydrates in Aqueous Solution. *J. Phys. Chem. A* **2001**, *105*, 10439−10445.

(20) Tsushima, S.; Yang, T.; Mochizuki, Y.; Okamoto, Y. Ab initio study on the structures of Th(IV) hydrate and its hydrolysis products in aqueous solution. *Chem. Phys. Lett.* **2003**, *375*, 204−212.

(21) Réal, F.; Trumm, M.; Vallet, V.; Schimmelpfennig, B.; Masella, M.; Flament, J.-P. Quantum Chemical and Molecular Dynamics Study of the Coordination of Th(IV) in Aqueous Solvent. *J. Phys. Chem. B* **2010**, *114*, 15913−15924.

(22) Spezia, R.; Beuchat, C.; Vuilleumier, R.; D'Angelo, P.; Gagliardi, L. Unravelling the Hydration Structure of ThX4 (X = Br, Cl) Water Solutions by Molecular Dynamics Simulations and X-ray Absorption Spectroscopy. *J. Phys. Chem. B* **2012**, *116*, 6465−6475.

(23) Hohenberg, P.; Kohn, W. Inhomogeneous electron gas. *Phys. Rev. B* **1964**, *136*, 864−871.

(24) Kohn, W.; Sham, L. J. Self-consistent equations including exchange and correlation effects. *Phys. Rev. A* **1965**, *140*, 1133−1138.

(25) Becke, A. D. Density-functional thermochemistry. III. The role of exact exchange. *J. Chem. Phys.* **1993**, *98*, 5648−5652.

(26) Roothaan, C. C. J. New Developments in Molecular Orbital Theory. *Rev. Mod. Phys.* **1951**, *23*, 69−89.

(27) Pople, J. A.; Nesbet, R. K. Self-consistent orbitals for radicals. *J. Chem. Phys.* **1954**, *22*, 571−572.

DOI: 10.1021/jp507613a
J. Phys. Chem. A 2015, 119, 689−703

(28) McWeeny, R.; Diercksen, G. Self-consistent perturbation theory. II. Extension to open shells. *J. Chem. Phys.* **1968**, *49*, 4852−4856.
(29) Perdew, J. P.; Chevary, J. A.; Vosko, S. H.; Jackson, K. A.; Pederson, M. R.; Singh, D. J.; Fiolhais, C. Erratum: Atoms, Molecules, Solids, and Surfaces - Applications of the Generalized Gradient Approximation for Exchange and Correlation. *Phys. Rev. B* **1993**, *48*, 4978−4978.
(30) Perdew, J. P.; Chevary, J. A.; Vosko, S. H.; Jackson, K. A.; Pederson, M. R.; Singh, D. J.; Fiolhais, C. Atoms, Molecules, Solids, and Surfaces: Applications of the Generalized Gradient Approximation for Exchange and Correlation. *Phys. Rev. B* **1992**, *46*, 6671−6687.
(31) Perdew, J. P.; Burke, K.; Wang, Y. Generalized gradient approximation for the exchange-correlation hole of a many-electron system. *Phys. Rev. B* **1996**, *54*, 16533−16539.
(32) Perdew, J. P., Unified Theory of Exchange and Correlation beyond the Local Density Approximation. In *Electronic Structure of Solids*; Ziesche, P., Eschrig, H., Eds.; Akademie Verlag: Berlin, 1991; pp 11−20.
(33) Burke, K.; Perdew, J. P.; Wang, Y. In *Electronic Density Functional Theory: Recent Progress and New Directions*; Dobson, J. F., Vignale, G., Das, M. P., Ed.; Plenum Press: New York, 1998.
(34) Seminario, J. M.; Araujo, R. A.; Yan, L. Negative Differential Resistance in Metallic and Semiconducting Clusters. *J. Phys. Chem. B* **2004**, *108*, 6915−6918.
(35) Seminario, J. M.; Derosa, P. A.; Cordova, L. E.; Bozard, B. H. A Molecular Device Operating at Terahertz Frequencies. *IEEE Trans. Nanotechnol.* **2004**, *3*, 215−218.
(36) Seminario, J. M. Calculation of intramolecular force fields from second-derivative tensors. *Int. J. Quantum Chem.* **1996**, *60*, 1271−1277.
(37) Rangel, N. L.; Sotelo, J. C.; Seminario, J. M. Mechanism of carbon-nanotubes unzipping into graphene ribbons. *J. Chem. Phys.* **2009**, *131*, 031105:031101−031104.
(38) Balbuena, P. B.; Calvo, S. R.; Lamas, E. J.; Salazar, P. F.; Seminario, J. M. Adsorption and Dissociation of H_2O_2 on Pt and Pt-alloy clusters and surfaces. *J. Phys. Chem. B* **2006**, *110*, 17452−17459.
(39) Aguilera-Segura, S. M.; Seminario, J. M. Ab Initio Analysis of Silicon Nano-Clusters. *J. Phys. Chem. C* **2014**, *118*, 1397−1406.
(40) Cárdenas-Jirón, G. I.; Leon-Plata, P.; Cortes-Arriagada, D.; Seminario, J. M. Electron Transport Properties through Graphene Oxide—Cobalt Phthalocyanine Complexes. *J. Phys. Chem. C* **2013**, *117*, 23664−23675.
(41) Salazar-Salinas, K.; Jauregui, L. A.; Kubli-Garfias, C.; Seminario, J. M. Molecular biosensor based on a coordinated iron complex. *J. Chem. Phys.* **2009**, *130*, 105101−105101−105109.
(42) Bobadilla, A. D.; Seminario, J. M. Assembly of a noncovalent DNA junction on graphene sheets and electron transport characteristics. *J. Phys. Chem. C* **2013**, *117*, 26441−26453.
(43) Rangel, N. L.; Seminario, J. M. Vibronics and Plasmonics Based Graphene Sensors. *J. Chem. Phys.* **2010**, *132*, 125102.
(44) Sotelo, J. C.; Yan, L.; Wang, M.; Seminario, J. M. Field Induced Conformational Changes in Bimetallic Oligoaniline Junctions. *Phys. Rev. A* **2007**, *75*, 022511 (022513 pages)..
(45) Rangel, N. L.; Seminario, J. M. Graphene Terahertz Generators for Molecular Circuits and Sensors. *J. Phys. Chem. A* **2008**, *112*, 13699−13705.
(46) Juaregui, L. A.; Seminario, J. M. A DNA sensor for sequencing and mismatches based on electron transport through Watson-Crick and non-Watson-Crick base pairs. *IEEE Sensors* **2008**, *8*, 803−814.
(47) Politzer, P.; Seminario, J. M. Energy Changes Associated with Some Decomposition Steps of 1,3,3-Trinitroazetidine - a Nonlocal Density-Functional Study. *Chem. Phys. Lett.* **1993**, *207*, 27−30.
(48) Habibollahzadeh, D.; Grodzicki, M.; Seminario, J. M.; Politzer, P. Computational Study of the Concerted Gas-Phase Triple Dissociations of 1,3,5-Triazacyclohexane and its 1,3,5-Trinitro Derivative (RDX). *J. Phys. Chem.* **1991**, *95*, 7699−7702.
(49) Politzer, P.; Seminario, J. M. Computational study of the structure of dinitraminic acid, $HN(NO_2)_2$ and the energetics of some possible decomposition steps. *Chem. Phys. Lett.* **1993**, *216*, 348−352.
(50) Murray, J.; Redfern, P.; Seminario, J.; Politzer, P. Anomalous Energy Effects in some Aliphatic and Alicyclic Aza Systems and their Nitro-Derivatives. *J. Phys. Chem.* **1990**, *94*, 2320−2323.
(51) Cao, X.; Dolg, M.; Stoll, H., Valence basis sets for relativistic energy-consistent small-core actinide pseudopotentials, *J. Chem. Phys.* **2003**, *118*.
(52) Cao, X.; Dolg, M. Segmented contraction scheme for small-core actinide pseudopotential basis sets. *J. Mol. Struct (THEOCHEM)* **2004**, *673*, 203−209.
(53) Hehre, W. J.; Ditchfield, R.; Pople, J. A., Self-consistent molecular-orbital methods. XII. Further extensions of Gaussian-type basis sets for use in molecular-orbital studies of organic-molecules, *J. Chem. Phys.* **1972**, *56*.
(54) Frisch, M. J.; et al. *Gaussian 09*, revision B.01; Gaussian, Inc.: Wallingford, CT, 2009.
(55) Peng, C.; Ayala, P. Y.; Schlegel, H. B.; Frisch, M. J. Using Redundant Internal Coordinates to Optimize Equilibrium Geometries and Transition States. *J. Comput. Chem.* **1996**, *17*, 49−56.
(56) Li, X.; Frisch, M. J. Energy-represented DIIS within a hybrid geometry optimization method. *J. Chem. Theory Comput.* **2006**, *2*, 835−839.
(57) Grimme, S.; Antony, J.; Ehrlich, S.; Krieg, H., A consistent and accurate ab initio parametrization of density functional dispersion correction (DFT-D) for the 94 elements H-Pu, *J. Chem. Phys.* **2010**, *132*.
(58) Barone, V.; Cossi, M. Quantum Calculation of Molecular Energies and Energy Gradients in Solution by a Conductor Solvent Model. *J. Phys. Chem. A* **1998**, *102*, 1995−2001.
(59) Cossi, M.; Rega, N.; Scalmani, G.; Barone, V. Energies, structures, and electronic properties of molecules in solution with the C-PCM solvation model. *J. Comput. Chem.* **2003**, *24*, 669−681.
(60) Roos, B. O.; Lindh, R.; Malmqvist, P.-Ã. k.; Veryazov, V.; Widmark, P.-O. New relativistic ANO basis sets for actinide atoms. *Chem. Phys. Lett.* **2005**, *409*, 295−299.
(61) Roos, B. O.; Lindh, R.; Malmqvist, P.-Å.; Veryazov, V.; Widmark, P.-O.; Borin, A. C. New relativistic atomic natural orbital basis sets for lanthanide atoms with applications to the Ce Diatom and LuF3. *J. Phys. Chem. A* **2008**, *112*, 11431−11435.
(62) Cao, X.; Dolg, M. Theoretical prediction of the second to fourth actinide ionization potentials. *Mol. Phys.* **2003**, *101*, 961−969.
(63) Ochterski, J. W.; Peterson, G. A.; J.A, M. J. A complete Basis Set Model Chemistry. V. Extensions to Six or More Heavy Atoms. *J. Chem. Phys.* **1996**, *104*, 2598−2619.
(64) Montgomery, J. A., Jr.; Frisch, M. J.; Ochterski, J. W. A Complete Basis Set Model Chemistry. VII. Use of the Minimum Population Localization Method. *J. Chem. Phys.* **2000**, *112*, 6532−6542.
(65) Montgomery, J. A., Jr.; Frisch, M. J.; Ochterski, J. W.; Petersson, G. A. A Complete Basis Set Model Chemistry. VI. Use of Density Functional Geometries and Frequencies. *J. Chem. Phys.* **1999**, *110*, 2822−2827.
(66) Pople, J. A.; Head-Gordon, M.; Fox, D. J.; Raghavachari, K.; Curtiss, L. A. Gaussian-1 theory: A general procedure for prediction of molecular energies. *J. Chem. Phys.* **1989**, *90*, 5622−5629.
(67) Curtiss, L. A.; Jones, C.; Trucks, G. W.; Raghavachari, K.; Pople, J. A. Gaussian-1 Theory of Molecular Energies Second-row Compounds. *J. Chem. Phys.* **1990**, *93*, 2537−2545.
(68) Curtiss, L. A.; Raghavachari, K.; Trucks, G. W.; Pople, J. A. Gaussian-2 theory for molecular energies of first- and second-row compounds. *J. Chem. Phys.* **1991**, *94*, 7221−7230.
(69) Curtiss, L. A.; Raghavachari, K.; Redfern, P. C.; Rassolov, V.; Pople, J. A. Gaussian-3 (G3) Theory for Molecules Containing First and Second-row Atoms. *J. Chem. Phys.* **1998**, *109*, 7764−7776.
(70) Curtiss, L. A.; Redfern, P. C.; Raghavachari, K. Gaussian-4 Theory. *J. Chem. Phys.* **2007**, *126*, 084108.
(71) Martin, J. M. L.; Oliveira, G. d. Towards Standard Methods for Benchmark Quality ab Initio Thermochemestry - W1 and W2 Theory. *J. Chem. Phys.* **1999**, *111*, 1843−1856.
(72) Allen, P. G.; Veirs, D. K.; Conradson, S. D.; Smith, C. A.; Marsh, S. F. Characterization of Aqueous Plutonium(IV) Nitrate Complexes by

DOI: 10.1021/jp507613a
J. Phys. Chem. A 2015, 119, 689−703

Extended X-ray Absorption Fine Structure Spectroscopy. *Inorg. Chem.* **1996**, *35*, 2841−2845.
(73) Wahlgren, U.; Moll, H.; Grenthe, I.; Schimmelpfennig, B.; Maron, L.; Vallet, V.; Gropen, O. Structure of Uranium(VI) in Strong Alkaline Solutions. A Combined Theoretical and Experimental Investigation. *J. Phys. Chem. A* **1999**, *103*, 8257−8264.
(74) Gaunt, A. J.; May, I.; Neu, M. P.; Reilly, S. D.; Scott, B. L. Structural and Spectroscopic Characterization of Plutonyl(VI) Nitrate under Acidic Conditions. *Inorg. Chem.* **2011**, *50*, 4244−4246.
(75) Johansson, G.; Magini, M.; Ohtaki, H. Coordination around thorium(IV) in aqueous perchlorate, chloride and nitrate solutions. *J. Solution Chem.* **1991**, *20*, 775−792.
(76) Moll, H.; Denecke, M. A.; Jalilehvand, F.; Sandström, M.; Grenthe, I. Structure of the Aqua Ions and Fluoride Complexes of Uranium(IV) and Thorium(IV) in Aqueous Solution an EXAFS Study. *Inorg. Chem.* **1999**, *38*, 1795−1799.
(77) Rothe, J.; Denecke, M. A.; Neck, V.; Müller, R.; Kim, J. I. XAFS Investigation of the Structure of Aqueous Thorium(IV) Species, Colloids, and Solid Thorium(IV) Oxide/Hydroxide. *Inorg. Chem.* **2002**, *41*, 249−258.
(78) Odoh, S. O.; Schreckenbach, G. Theoretical Study of the Structural Properties of Plutonium(IV) and (VI) Complexes. *J. Phys. Chem. A* **2011**, *115*, 14110−14119.
(79) Spezia, R.; Jeanvoine, Y.; Beuchat, C.; Gagliardi, L.; Vuilleumier, R. Hydration properties of Cm(III) and Th(IV) combining coordination free energy profiles with electronic structure analysis. *Phys. Chem. Chem. Phys.* **2014**, *16*, 5824−5832.
(80) Bühl, M.; Kabrede, H.; Diss, R.; Wipff, G. Effect of Hydration on Coordination Properties of Uranyl(VI) Complexes. A First-Principles Molecular Dynamics Study. *J. Am. Chem. Soc.* **2006**, *128*, 6357−6368.
(81) Tsushima, S.; Yang, T. Relativistic density functional theory study on the structure and bonding of U(IV) and Np(IV) hydrates. *Chem. Phys. Lett.* **2005**, *401*, 68−71.
(82) Atta-Fynn, R.; Johnson, D. F.; Bylaska, E. J.; Ilton, E. S.; Schenter, G. K.; de Jong, W. A. Structure and Hydrolysis of the U(IV), U(V), and U(VI) Aqua Ions from Ab Initio Molecular Simulations. *Inorg. Chem.* **2012**, *51*, 3016−3024.

DOI: 10.1021/jp507613a
J. Phys. Chem. A 2015, 119, 689−703